Miniature Self-Contained Intravascular Magnetic Resonance (IVMI) Probe for Clinical Applications

Aharon Blank,[1]* Gil Alexandrowicz[1,4] Lev Muchnik,[1]
Gil Tidhar,[1] Jacob Schneiderman,[2] Renu Virmani,[3] and Erez Golan[1]

A miniature (1.73 mm in diameter) NMR probe, which contains a magnet and a radiofrequency (RF) coil, is presented. This probe is integrated at the tip of a standard catheter and can be inserted into the human coronary arteries, creating local magnetic fields needed to obtain the NMR signal from the blood vessel walls, without the need for external magnet or RF coils. The basic theory governing the probe performance in terms of signal-to-noise-ratio and contrast parameters is presented, along with measured results from test samples. The NMR signal can be analyzed to obtain tissue contrast parameters such as T_1, T_2 and the diffusion coefficient, which may be used to detect lipid-rich vulnerable plaques in the coronary arteries. Magn Reson Med 54:105–112, 2005. © 2005 Wiley-Liss, Inc.

Key words: NMR; MRI; inside-out; ex situ; vulnerable plaque

NMR and its descendant, MRI, are usually pursued in a setup based on a highly homogenous static magnetic field, B_0, with variance <1 ppm, creating nuclear spin precession at a corresponding narrow band of frequencies (1,2). The homogeneous static field setup has several advantages such as the ability to obtain chemical shifts, while ensuring good signal-to-noise-ratio (SNR) due to the small bandwidth involved. However, this setup suffers from the need to employ large magnets that usually surround the examined sample/object. In more specific cases, such as clinical MRI systems, the large magnet, and the corresponding large radiofrequency (RF) and gradient coils are a major factor in the relative complexity and the high cost of such systems. If one is interested only in a specific small region within the body, it could be highly advantageous to obtain NMR information by using either a noninvasive hand-held probe or an intracavity self-contained (magnet + RF and gradient coils) NMR probe, thus avoiding the requirement for a large external magnet. Such an approach for NMR measurement or NMR imaging without a sample-surrounding magnet is termed "inside-out," or ex situ (3–7). Using the inside-out setup it is usually impossible to create highly homogeneous fields outside the magnet. Several types of systems that operate in an inside-out geometry were designed and built, demonstrating measurement capabilities of relaxation parameters (8,9), diffusion coefficients (10), spectroscopic data (11), and a capability of 3D imaging (12). In the case of microscopic MRI, where very high field gradients are required to obtain high resolution, inside-out systems were found very useful and enabled the acquisition of images with a resolution of about 1 μm, outside a superconducting magnet (5,13), or near a fine magnetic tip (14,15).

The efforts described above were mainly directed toward materials science applications or related subjects, with appreciable achievements. However, until now there has been no demonstration of the full potential of this method to approach clinically significant problems, for which current MRI systems cannot provide an answer due to limitations in resolution, SNR, gradient magnitude, complexity, local measurement flexibility, and even cost. The unavailability of such a demonstration is probably due to the extreme difficulties that the inside-out methodology brings with it (as discussed below), which must be resolved prior to realizing any clinical application. In the present paper, a significant step toward clinical capability is presented by means of a new type of self-contained (magnet + RF coil) inside-out NMR probe. The probe is intended for intravascular clinical use. The advantages of this technique range from the very practical aspect of a low-cost system (since no expensive external setup is required) to accessibility to the patient during the procedure, compatibility with existing interventional tools, and finally resolution and diffusion contrast measurement capabilities that are superior to conventional clinical MRI (due to the strong local gradients created by the NMR probe and its proximity to the examined tissue). The probe has undergone an extensive set of tests including bench tests in phantoms, ex vivo human heart measurements, in vivo animal trials, and in vivo human clinical studies. This article discusses the physical layout of the probe and its principles of operation and presents some of the bench tests results. The ex vivo results in human coronary arteries are described in a complementary paper (16). The intravascular probe serves as a first example for a wide range of applications for this method, which in the near future may open new possibilities to the field of clinical MRI.

Before describing the probe and the experimental results, a brief description of the field of interventional cardiology and intracoronary arteries imaging is given. This medical field was chosen as the first application for this novel approach. New data obtained over the past 10 to 15 years suggests that the paradigm that acute coronary syn-

[1]Topspin Medical (Israel), Ltd., Global Park, Lod, Israel.

[2]Department of Vascular Surgery and Gottesdiener Vascular Biology Laboratory, Sheba Medical Center, Sackler Faculty of Medicine, Tel Aviv University, Tel Aviv, Israel.

[3]CV Path, International Registry of Pathology, Gaithersburg, Maryland, USA.

Present address for Gil Alexandrowicz: 413c PCS Surface Physics Group, Cavendish Laboratory, Madingley Road, Cambridge CB3 0HE, United Kingdom.

Present address for Lev Muchnik: Department of Physics, Bar Ilan University, Ramat-Gan 52900, Israel.

*Correspondence to: A. Blank at present address: B-27 Baker Lab, Department of Chemistry and Chemical Biology, Cornell University, Ithaca, NY 14853, USA. E-mail: ab359@cornell.edu

Received 11 October 2004; revised 3 February 2005; accepted 3 February 2005.

DOI 10.1002/mrm.20537
Published online in Wiley InterScience (www.interscience.wiley.com).

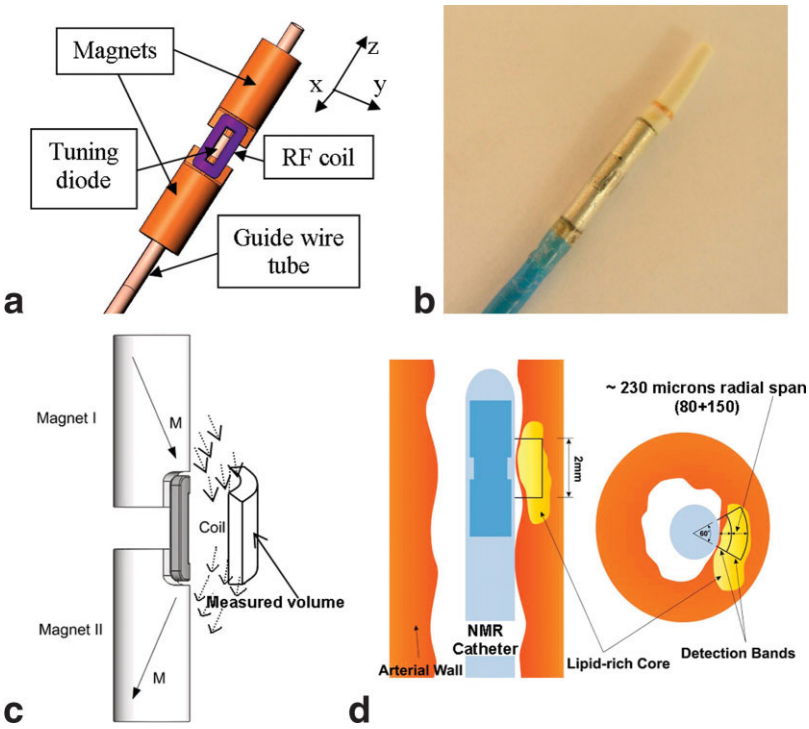

FIG. 1. (**a**) A drawing of the miniature self-contained "inside-out" NMR probe. The diameter of the probe is 1.73 mm and its height (defined by the magnets) is 10 mm. The RF coil is made of an enameled bondable 22-μm copper magnet wire (80 windings) placed between the permanent magnets. It has elliptical shape as shown in the drawing with height of 1.5 mm, width of 1 mm, and thickness of 0.2 mm. The inductance of the coil is ~18 μH and its DC resistance is ~ 25 Ω, while at 10 MHz it is ~100 Ω (due to the skin effect). The resulting static field is predominantly along the *z*-axis, and the RF field is mainly along the *x*-axis in the measured region, which is located just in front of the RF coil. (**b**) Photograph of the probe inside the catheter tube showing the aluminum coating (see text). The balloon (not shown) is located at the "rear" of the probe, opposed to the coil side (see text). (**c**) A different view of the probe components showing the direction of magnetization (the magnets are magnetized at an angle of ±45° with respect to the probe *z*-axis) and the approximate measured region in front of the probe, which is limited in its radial, angular, and longitudinal extent (see text). Magnetic flux lines are plotted as small dotted arrows. (**d**) A cartoon showing the method of signal acquisition with the probe inside the blood vessel.

dromes (ACS), including heart attacks, are caused by gradual narrowing of coronary arteries is not accurate. It is known today that more than 70% of heart attacks are caused by sudden rupture or erosion of vulnerable coronary plaques that are only moderately (<50%) narrowed, prior to the formation of an occluding thrombus. Such vulnerable plaque (VP) rupture is now known to happen in coronary segments that contain a large lipid-rich necrotic core making up more than 40% of the arterial cross-section, covered by a thin (<100 μm) fibrous cap (17). In most cases inflammatory processes play an important role in the mechanical weakening of the fibrous cap, thereby accelerating the rupture process in VPs (18). The ability to detect VPs before they rupture in order to allow the interventional cardiologist to treat them and prevent subsequent ACS is currently one of the most important missions of medical imaging. Current imaging modalities are limited, either in resolution (e.g., MRI) or in tissue characterization capability (e.g., ultrasound and optical coherence tomography) (19). The probe developed and presented here is aimed at addressing this challenge.

METHODS AND THEORY

In this section the new NMR probe is described in detail, including its basic components, materials, method of construction, and field profiles. Following that, theoretical calculation of the NMR signal, in the context of the new probe, is given.

The NMR Probe

A schematic drawing and a photograph of the NMR probe are given in Fig. 1. The dimensions of the probe are designed to enable its maneuvering in the tree of the coronary arteries. For such a small-diameter probe, the magnetic field can be generated efficiently only by means of a strong permanent magnet (Vacodym-722-AP from Vacuumschmelze, Germany, having energy density BH_{max} of about 417 kJ/m^3 and remanent B_r of about 1.36 T), and not by a miniature electromagnet. The magnets, which are made of moderately conductive anisotropic ceramic material, can be machined to their required shape by conventional spark and wire erosion. The resulting calculated and measured static magnetic fields of the probe are given in Fig. 2a. The field is strongest near the coil and is not axis-symmetric due to the asymmetric nature of the magnetization direction of the magnet pair (Fig. 1c) and the asymmetric shape of the magnets. The gradient that results from such a small configuration is in the range of 150–200 T/m and may be controlled to some extent by changing the angle of the magnetization and the dimensions of the gap between the two magnet pieces (Fig. 1c). Thus, when the magnetization vector **M** is closer to being parallel to the probe axis (*z*-axis), the gradient in the measured volume of interest becomes larger. Similarly, reducing the gap between the magnets also increases the gradient. The existence of a gap also minimizes the effects of eddy currents (20,21) that may be generated in the conductive magnet (conductivity $\sigma \sim 5 \times 10^5$ S/m) and also reduces potential problems due to magnetoacoustic ringing (22) that are typical for cases where the coil and the conductive magnet are in close proximity. Due to volume constraints, a single coil is used both for transmission and for reception. The calculated and measured B_1/I of the coil (the RF field generated when 1 A of current flows through the coil) are given in Fig. 2b.

Due to its small size and the steep radial fall-off of its static and RF magnetic fields, the probe can obtain the

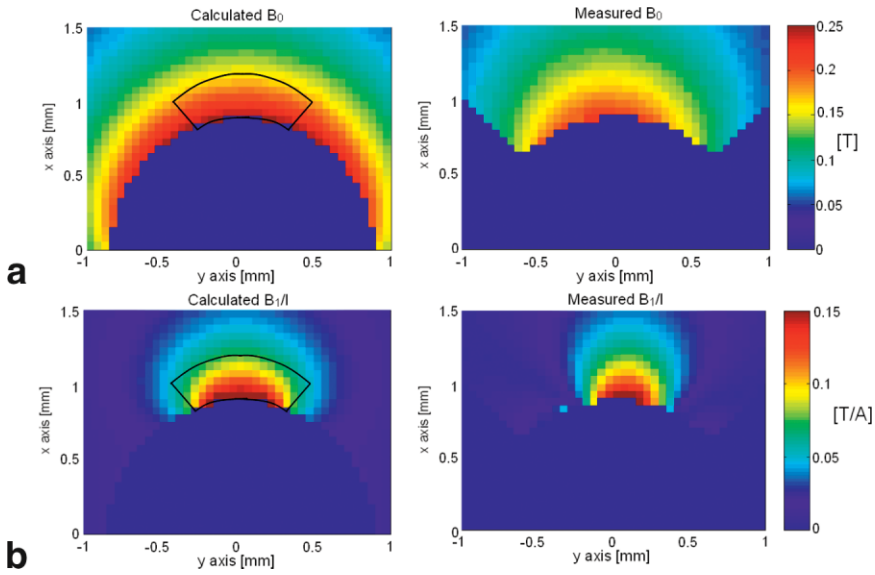

FIG. 2. (**a**) Calculated and measured B_0^z of the probe at the plane $z = 0$. The calculations were performed with Maxwell finite element software (Ansoft) and the measurements were obtained by computerized 3D scanning of a miniature Hall probe (Model 3RT100–2-2–0.2T, Sentron, Switzerland) around the magnet. The Hall probe measures the 3D field vector from a very small integrated volume of 100 × 100 × 100 μm. (**b**) Calculated and measured B_1^x/I of the RF coil at the plane $z = 0$. The calculations were performed by numerical integration along the coil path using Biot–Savart law. The measurements were performed with the same Hall probe employed for the static field measurements, but at a frequency of 100 Hz. Due to measurement limitations, one cannot obtain the fields in all calculated points. The region from which the NMR signal is obtained (black lines) is superimposed on the calculated plots.

NMR signal only from a very limited and specific volume of interest (cf. Figs. 1c and 2). This limited volume, however, is sufficient for clinical operation where the probe is in contact with the inner boundary of the blood vessel (16) and has to obtain a signal only from a limited region (typically 250 μm) going into the blood vessel wall (17). The unique static magnetic field profile created by this inside-out probe at the measured volume is significantly different from that created by conventional NMR or MRI setups. This static field profile results in typical system characteristics, which are very different from those of standard NMR or MRI machines. For example, the required bandwidth of the system, relative to the center frequency of operation, is very large since the required imaging region, spanning ~0–250 μm from the probe (17), corresponds to a total bandwidth of ~2.5 MHz around a center Larmor frequency of ~9 MHz (Fig. 2). For practical transmitter power, the entire bandwidth of interest cannot be covered efficiently with a single center-frequency hard pulse (23). Rather, the measured region should be divided into frequency bands (2 bands of ~1.3 MHz in the present probe design), which are excited separately by a selective pulse (see Fig. 3). Another challenge is the low baseline SNR. For example, in order to obtain signal only from the vulnerable plaque's fibrous cap, the radial dimension of the closest measured voxel (extending away from the probe, see Fig. 4) should be ~80 μm (16,17). This requirement leads to a very small volume of spins and therefore to a very low signal level. At the same time, the bandwidth of the 80-μm voxel is ~1.3 MHz, giving rise to significant thermal noise.

To increase the number of averaged echoes as much as possible and to minimize signal decay due to diffusion (see below), the system must have very short dead time between RF pulse transmission and echo signal reception. Achieving short dead time ($\tau < 6$ μs) with ~100 V transmission pulses over the long CPMG sequence (Fig. 3), and for relatively low RF frequency (~9 MHz), requires a multistage passive and active duplexer system. The duplexer system that was constructed (described schematically in Fig. 5) achieved a dead time of ~4.5 μs with reasonable noise figure of 2 dB for the entire bandwidth of operation. This short dead time is superior to that achieved in previous experiments, performed under similar conditions (31). A block diagram of the major system components is shown in Fig. 6.

In contrast to clinical MRI systems, which can operate efficiently only in an RF shielded room, the inside-out probe should be operated in conventional unshielded catheterization labs. This poses major noise problems that can potentially degrade the probe performance. Fortunately, the potential difficulties can be solved by taking advantage of the unique "inverted" geometry of the inside-out probe. This is achieved by vacuum deposition of a thin layer of aluminum on the probe (Fig. 1b), which effectively shields out noise disturbances coming from the outside

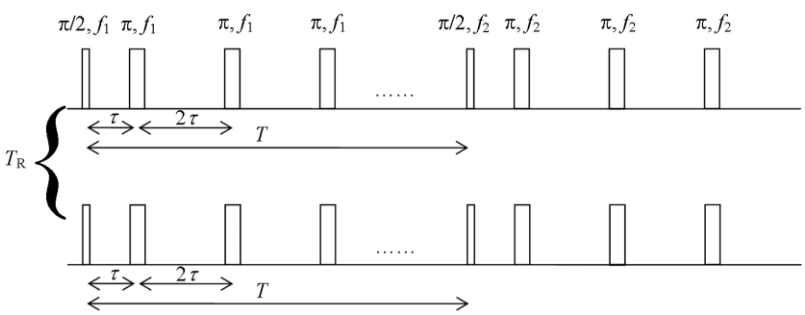

FIG. 3. An example for a pulse sequence employed by the NMR probe. Typically $\tau = 5$ μsec, 1000 pulses are produced in the CPMG train, $T = 100$ msec, and $T_R = 300$ msec. Since the typical T_2 of the tissue is ~30–50 ms (34), which is much shorter than T_1, one can cover the entire bandwidth of interest during a single T_R by several CPMG trains at different excitation frequencies (f_1, f_2, etc.). Averaging for a typical period of 40 s enables the accumulation of ~135000 echoes, which improves the single shot SNR by a factor of ~365.

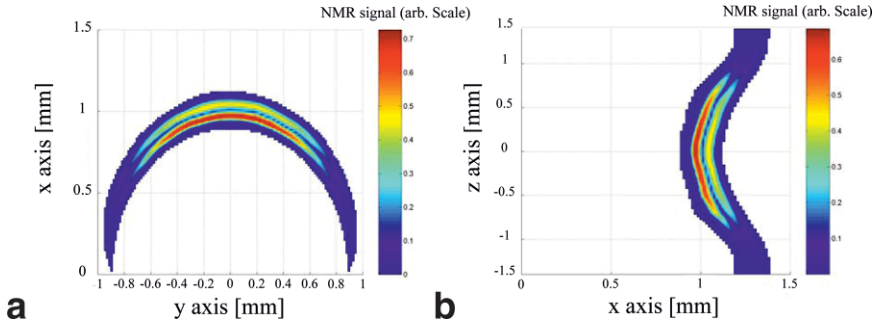

FIG. 4. Spatial distribution of the NMR signal from the measured region, as calculated using the method described in Ref. (29). (**a**) The signal in the *xy* plane; (**b**) the signal in the *xz* plane. Two regions of excitation are clearly visible, corresponding to the two frequencies of excitations employed by the probe (8 and 9.5 MHz). The spatial resolution of the measurement is determined for the *z*- and the *y* (angular) axis, mainly by the size of the coil, while the x-axis (radial) resolution is determined by the excitation bandwidth and the curvature of the magnetic field. The single-shot SNR for the two excited bands was calculated to be 0.12 and 0.07, respectively.

(that can be characterized mainly as plane electromagnetic waves). On the other hand, such a thin layer still enables the transmission with small losses (~1 dB) of the spherical wave of the RF magnetic field coming from the coil (excitation pulses) and those coming back to the coil from the precessing spins (24). The shield in the present probe was found efficient when used in patients despite the fact that the human body tends to couple noise interferences to objects inserted into it (25,26).

To facilitate the clinical function of the NMR probe, it was encapsulated inside the distal tip of a 1.73-mm outer-diameter catheter. The probe is electrically connected to the external console by a coax cable (Model PCX40K10 from Axon, France) running through the catheter (Fig. 6). The catheter itself can be navigated into and inside the coronary arteries over a 0.014-inch conventional guidewire, through an 8-Fr guiding catheter. A gentle side balloon located adjacent to the NMR probe can be inflated during signal acquisition in order to stabilize the catheter and ensure good SNR for the high-resolution measurements. It should be emphasized that the ability to stabilize the magnetic fields with respect to moving tissue, and thus to average the signal efficiently over many seconds of acquisition, is a major advantage of the self-contained NMR configuration. Conventional MRIs produce field gradients from the outside and therefore cannot ensure stationary static (B_0 + gradient) fields in a moving tissue, unless gating techniques are used (which reduce the effective signal acquisition time and in turn the SNR and spatial resolution). More details regarding the clinical procedure appear in Ref (16).

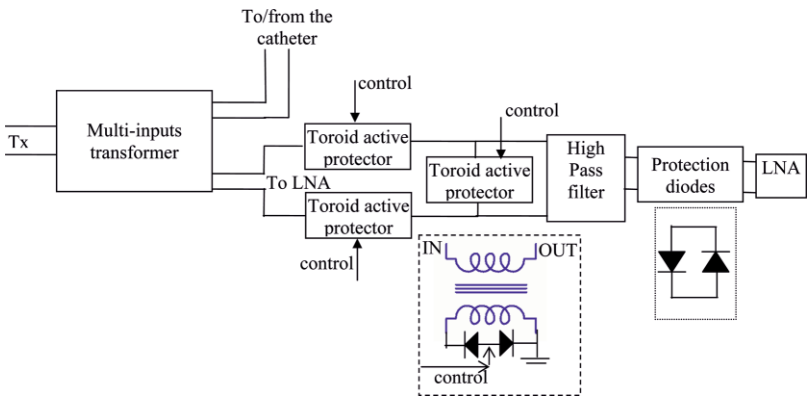

FIG. 5. Block diagram of the duplexer circuit. During the transmission, high-voltage RF pulses coming from the transmission line are coupled to the RF coil in the catheter through a multi-inputs RF transformer. The transmission pulses are also coupled to the line going to the LNA, but with reduced voltage, due to a favorable turn ratio in the transformer. The residual voltage coming out of the transformer to the LNA during transmission is attenuated with active toroid protectors (one specific design is shown here surrounded by a dashed box (35)). Each toroid protector has primary and secondary turns, where the signal goes through the primary turns and the secondary can either be shorted out, by means of PIN diodes, or provide an open circuit. When the secondary is shorted out the primary of the toroid shows low RF impedance and the signal passes through easily. The opposite holds when the secondary exhibits an open circuit. The toroid protectors that lie in series to the signal lines exhibit high RF impedance during transmission, while the toroid protector that is in parallel to the lines exhibits RF low impedance during transmission (the opposite holds for reception mode). Following the toroid protectors is a passive high-pass filter to remove any DC or low-frequency bias that may be generated during the high-voltage pulses. Finally, just before the LNA there are low junction voltage Schottky diodes (shown here in the dotted box) that protect the LNA directly and limit the maximum voltage in its input.

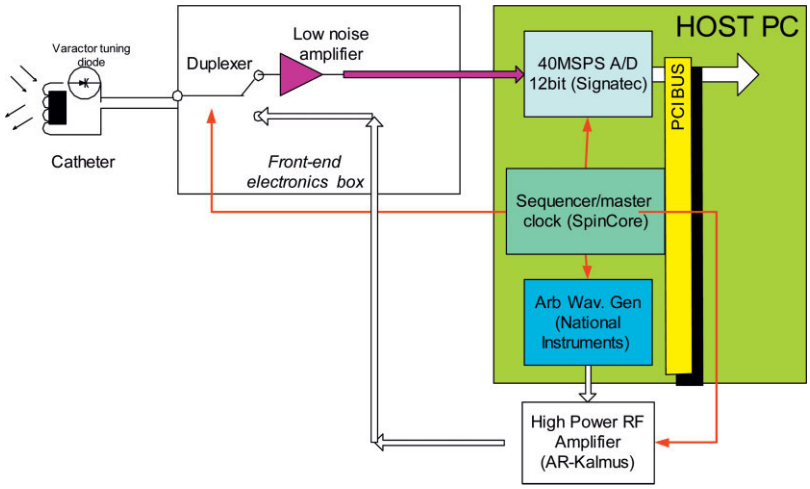

FIG. 6. Block diagram of the imaging system. A host PC initiates a pulse sequence within the master clock (Model 50–24 SpinCore, FL). Each timing pulse results in an appropriately shaped RF pulse by means of the arbitrary waveform generator (Model NI 5411 from National Instruments). The RF pulses are being amplified (1 kW amplifier from Kalmus/AR) and then pass through a duplexer (Fig. 5) to the coil in the catheter. The returned echo signal is picked up in the resonant coil (its resonance frequency is controlled via a varactor diode) and goes back through the duplexer to a low noise amplifier, sampled in the A/D card (model PDA14 from Signatec) in the PC, where the signal is processed to provide the tissue contrast parameters.

Theory of Operation

Having described the probe and the NMR system, we now turn to a more quantitative discussion regarding the theory governing the probe performance: The single shot SNR, assuming proton density as in water, is given by (27)

$$SNR = \frac{9.3 \times 10^5 \cdot B_0^2 \cdot (B_1/I) \cdot \Delta V}{\sqrt{4k_b \cdot T \cdot \Delta F \cdot R \cdot NF}}, \qquad [1]$$

where (B_1/I) is the sensitivity of the pickup coil as described above, ΔV is the excited volume, k_b is Boltzmann's constant, T is the temperature, ΔF is the bandwidth of the receiver, and R is the pickup coil resistivity. Here it is assumed that the amplification stage has noise figure of NF (the ratio of the output SNR to the input SNR). As noted above, in any inside-out scenario, B_0 and B_1 vary significantly within the excited volume of interest and a numerical calculation must be performed to obtain the exact signal amplitude (28,29). Although Eq. [1] is an approximation, (for the finite volume with varying B_0 and B_1) it is useful to provide a rough estimate of the SNR performance. The volume of the measured spins can be approximated by means of the coil dimensions in the z and y directions (Fig. 1), which are 1.5 and 1 mm, respectively, and by the sampling resolution (~100 μm) in the x direction. For typical B_0 of 0.2 T, (B_1/I) of 0.06 T/m (in the rotating frame), ΔV of 1.5×10^{-10} m^3, and temperature of 37°C, one obtains a typical single-shot SNR of 0.11 (NF = 2). A more accurate numerical calculation, employing the method described in Ref. (29), provides the exact sensitive volumes (Fig. 4). This numerical calculation provides single shot SNR of 0.12 and 0.07 for the imaged voxels centered at a distance of ~35 and ~140 μm away from the probe surface and spanning ~80 and ~150 μm in the x-axis, respectively (Fig. 4). Due to this relatively low single-shot SNR, one must employ an extensive averaging scheme to further increase it by means of repeated CPMG sequences, as shown in Fig. 3 (28,30). At distances beyond ~400 μm the averaging time is too long for clinical applications (typically it should be not more than 40 s in the present probe configuration, due to partial occlusion of the blood vessel by the inflated balloon). Fortunately, most of the relevant clinical information lies at distances smaller than 250–300 μm from the edge of the probe (17).

As mentioned briefly above, the large static field gradients of the probe can cause a severe decrease of the NMR signal. This is due to the fact that under the extremely large field gradients in the measured region, the echo decay in the CPMG train is strongly affected by the self-diffusion of the nuclear spins. Again, for inside-out probes, an exact description of this phenomenon requires rather involved numerical calculations (28,29). Nevertheless, for the sake of the present discussion, good approximate results are given by the equation (23)

$$A(m) = e^{-(mt)/\tau_2} \cdot \exp\left(-\frac{2}{3}\gamma^2 G^2 D\tau^2(m\tau)\right) \qquad [2]$$

where m is the index of the echo in the CPMG train, τ is the separation between the 90° and 180° pulses (which are certainly not perfect for the inside-out case (28)), γ is the nuclear gyromagnetic ratio, G is the gradient, and D is the diffusion coefficient. Equation [2] shows that the echo decay along the CPMG train is dominated by diffusion effects (for large τ) or by T_2 effects (for short τ). This statement can be made more quantitative: To have a more or less equal contribution to $A(m)$ from diffusion and T_2 effects, in the present configuration ($G \sim 200$ T/m), one requires that the echo decay in water-like tissue ($D = 10^{-9}$ m^2/s) over 10 ms will not exceed ~50% (assuming a typical water T_2 of ~30 ms). In view of Eq. [2], this requirement implies that τ should be shorter than ~6 μsec, as was indeed achieved with the duplexer of the present system (Fig. 5). The capability to employ even shorter τ enables one to obtain (for water-like tissue) either a predominantly T_2 weighted echo decay ($\tau < 6$ μs), or a D-weighted echo decay ($\tau > 6$ μs), at will.

RESULTS AND DISCUSSION

As an initial step to verify the performance of the probe, the single-shot SNR was measured and compared to the calculated results (see above and also Fig. 4). The measurements were performed by dipping the catheter probe in a

mixture of 70% water and 30% glycerol, at 25°C (which has similar $D \sim 0.5 \times 10^{-9}$ m^2/s and $T_2 \sim 30$ ms characteristics to that of a typical lipid rich nectrotic core (16), at the probe static magnetic field). The CPMG sequence, shown in Fig. 3, was employed with $\tau = 5.5$ μs and $T_R = 0.6$ s (much larger than T_1). Each echo in the train is sampled at several points (acquisition bandwidth of 40 MHz) and the peak of the Fourier transform of this time-domain signal is taken as the echo signal (for each echo in the train). The sequence was repeated 2000 times and, for single-shot SNR measurements, the average of only the first echo in the train was considered. The SNR of this averaged echo was found to be 4.5 and 2.7 for the first and second measured voxles, respectively (Fig. 4), which translates to a single-shot SNR of 0.1 and 0.06, respectively (after dividing by $\sqrt{2000} = 44.7$). This is in good agreement with the calculated single-shot SNR results of 0.12 and 0.07 for the first and second measured voxles, respectively (Fig. 4). A much higher SNR is obtained by averaging all the echoes in the train, in addition to the averaging along the T_R axis (Fig. 3). Thus, in the case of 70% water and 30% glycerol ($D \sim 0.5 \times 10^{-9}$ m^2/s), for $\tau = 5.5$ μs, the echo decay after 1000 echoes is only ~15% (Eq. [2]), and considering all these echoes can enhance the SNR substantially. The measured SNR after 40 s of acquisition, when averaging these 66000 (= 1000 × 40/0.6) echoes to a single result, was 22.5 and 14 for the two volumes of excitation (Fig. 4), again in good agreement with the calculations.

An additional important parameter that was verified during the bench tests is the radial resolution of the probe. This was carried out by measuring the signal in the two excitation bands with the same probe for several different types of outer-layer coatings. Sequential addition of these coatings (made of thin heat shrink plastic tubes) causes a gradual increase in the distance between the probe and the water/glycerol mixture, thereby making it possible to know the distance to the region excited by each band. A summary of these measurements is given in Fig. 7. The first band (9.5 MHz) gets its signal mainly from the first ~70 μm near the probe, while the second band gets its signal mainly from a radial distance of ~60–200 μm from the probe. These measurements are in good agreement with the predictions (Fig. 4).

After the signal has been acquired with sufficient SNR, one must analyze it to obtain the image contrast that would enable the possible diagnosis of the existence of vulnerable plaque. Basically, three types of contrasts can be extracted from the measured data, namely T_1, T_2, and/or D. It was most useful to differentiate between the lipid-rich necrotic core and the fibrotic tissues by means of the apparent diffusion coefficient (16,32). This parameter is quantified through the characteristic decay time, T_c, of the echo signals along the CPMG train, which is a function of the tissue T_2 and D, and the probe/system parameters G and τ (Eq. [2]). Thus, for a typical $\tau = 5.5$ μs, the lipid pool is characterized by $T_c \sim 15$ ms, and the fibrotic tissue has $T_c \sim 4.5$ ms (16,32). We have verified in our bench tests the capability to accurately differentiate between different T_c's during the 40 s available for clinical measurements. This was done with two samples having different characteristic echo decay times, as shown in Fig. 8. These results show

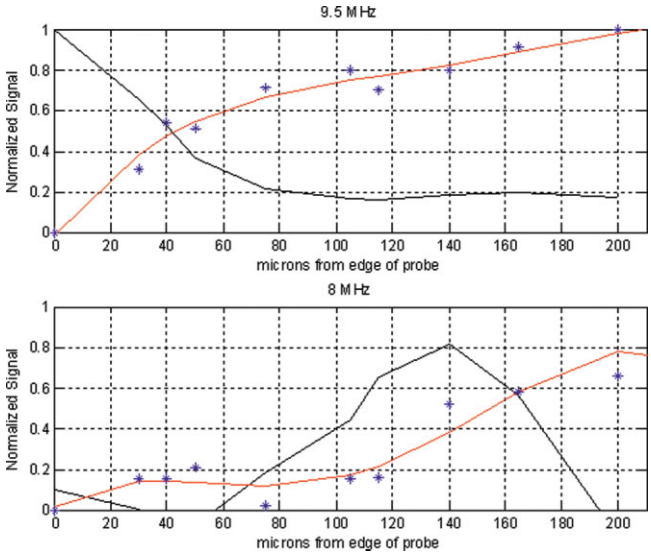

FIG. 7. The NMR signal as a function of the radial distance from the probe for the two frequencies of excitation. The experimental points (stars) represent the decrease in the measured signal as coatings are added to the probe. Thus, for example, at the origin, without applying any additional coatings on the probe, the measured signal for both measured regions (excited at 8 and 9.5 MHz) is maximal and the measured signal decrease is 0. As one adds additional coatings to the probe, the measured signal from the two regions of excitation becomes smaller, and the measured signal decrease becomes larger. A polynomial fit (solid red line superimposed on the experimental points) was used to extract the functional behavior of this measured signal decrease. The solid red line is thus the cumulative distribution of the NMR signal as a function of the radial distance. In other words, the red line corresponds to the measured signal, assuming that instead of adding coatings to a probe dipped in liquid, one would have added layers of liquid around a probe placed in the air (which is experimentally not practical and that is why we employed the present method of measurement, with this particular measured signal decrease terminology). The derivative of this line (black solid line) represents the signal distribution as a function of radial distance from the probe edge, which is the information of importance extracted from this type of experiment.

that the probe has enough SNR (for such short measurement time) to identify with high precision the characteristic echo decay time and to enable tissue characterization with fine radial resolution that can potentially allow VP identification (16) in the future. In addition, the high spatial radial resolution (~70 μm) of the first excited volume, which is adjacent to the inner boundary of the vessel wall, enables one to estimate the distance of the lipid pool from the lumen with high precision and thus provides good assessment of the vulnerability of this lipid pool (16,17).

Given its high lipid-specific tissue characterization capability, high spatial resolution along the radial dimension, and voxel conformity to the lumen, the probe should be superior to clinical MRI for this application. Thus, while conventional MRI can obtain images of the coronary arteries in a rectangular grid with ~0.46-mm planar resolution and ~2- to 5-mm slice thickness (33), the present probe obtains the signal in a cylindrical-type grid (that is more suitable for blood vessels), with z resolution of ~1.5 mm, angular resolution of ~60°, and radial resolu-

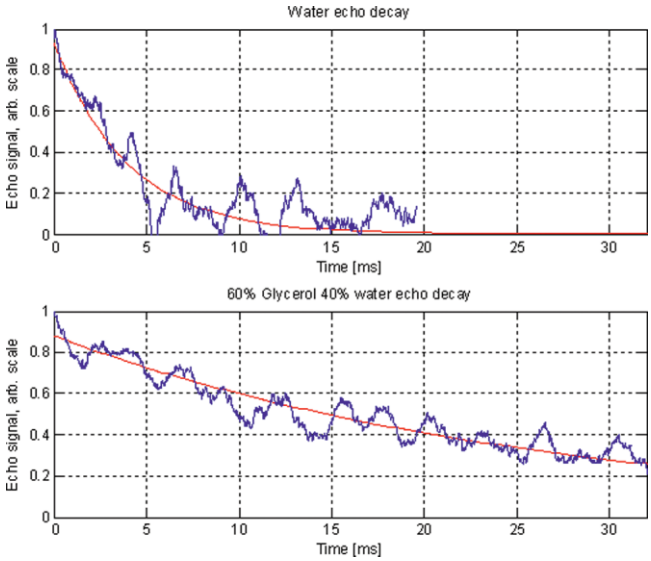

FIG. 8. Typical echo decay plots used to characterize the type of sample measured. Measurements were performed with the NMR probe at 9.5 MHz with $\tau = 5.8$ μs for a period of 40 s. The upper plot shows the 1800 echoes measured for a water sample, which has characteristic echo decay time, T_c, of 4 ± 0.4 ms (the superimposed red line), due to its relatively large diffusion coefficient. The lower plot shows the 3000 echoes measured for sample of 60% glycerol and 40% water. Here the characteristic decay time is 26 ± 5.2 ms. Each point represents a moving window average over 100 echoes.

tion of 70–150 μm. On the other hand, the intravascular probe is by definition invasive and has a limited field of view compared to conventional cardiac MRIs. Thus, we envision this novel technique as an important real time complement to cardiac MRI or multislice CT for diagnosing coronary plaque during cardiac catheterization. Future developments may allow the combination of several measurements at different angular positions as well as at different longitudinal positions along the artery to reconstruct a three-dimensional image of the vessel wall. Each measurement obtains the signal for a limited angular and longitudinal blood vessel wall segment (Fig. 1d). Different sectors of the blood vessel can be measured by a combination of longitudinal movement of the probe and rotation around its guide wire. We provide here (Fig. 9), just for reference, representative results from such multisite measurement, as obtained in recent ex vivo experiments (16). It shows qualitatively the capability of differentiating between areas of low and high T_c and identifying the distance of these areas from the lumen of the blood vessel.

SUMMARY AND CONCLUSIONS

A new approach to clinical NMR measurements has been presented, directed at the diagnosis of coronary VP, which is currently an "open problem" for the current diagnostic or imaging modalities. System performance has been analyzed using theoretical predictions and measured bench test results. The capability of diagnosing VP in a clinical setting is currently being validated both by a series of ex vivo experiments (16) and in human clinical studies. The methodology developed here can be extended to other applications in medicine and beyond. Scaled-up versions of the NMR probe can be designed for applications where local NMR information of an adjacent tissue or organ is needed and specifically where conventional MRI systems

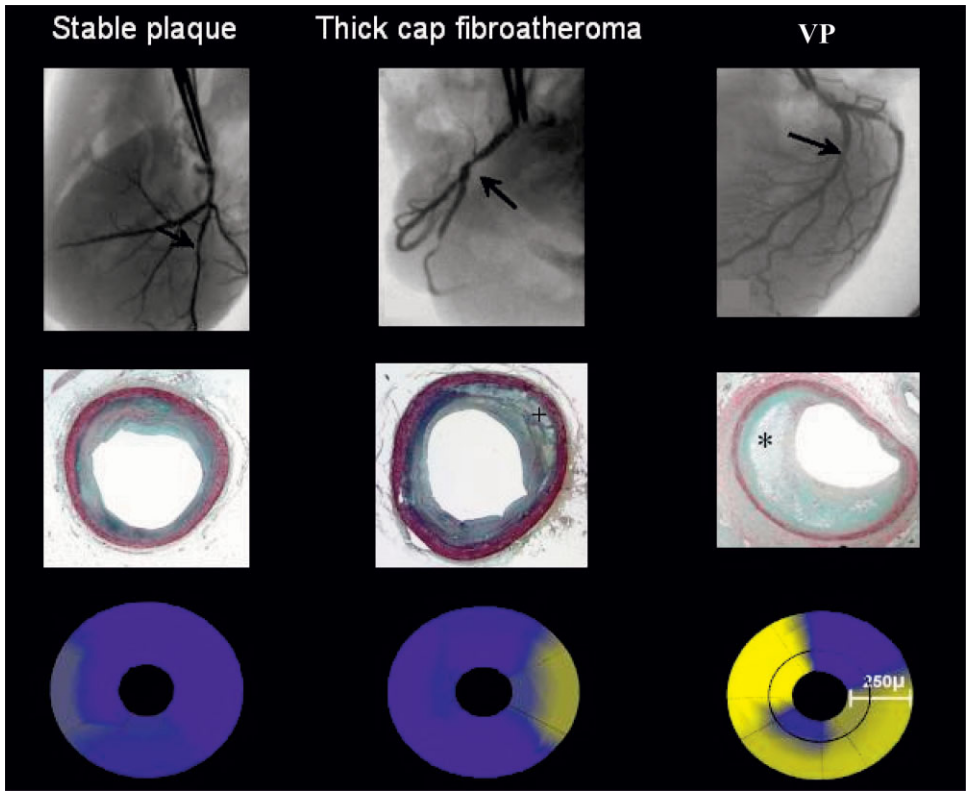

FIG. 9. Example of the qualitative apparent diffusion coefficient (T_c) in a "multisite" probe measurement of an ex vivo heart (adapted from Ref. (16)). The color scale (blue/yellow) corresponds to short/long T_c. The measurements show results from three different sites, where in each site two radial bands were measured in four quadrants. On the left one can see a stable plaque, where T_c all over is short. In the center one can see an area of lipids, but it is distant enough from the lumen, and thus it is not considered a potential problem. On the right one can see typical VP, where the lipid-rich necrotic core is very close to the lumen.

cannot be practically used. If the probe is more than a few millimeters in diameter, it may allow the inclusion of gradient coils for better resolution. One such example is the use of a transrectal NMR probe for imaging the prostate gland. The SNR considerations given here can be used to demonstrate that a larger transrectal probe can be designed to give a field of view of a few centimeters into the prostate, allowing for potential use in diagnosing prostate cancer, guidance of biopsy needles, and staging. Utilizing this method in such applications is not intended to replace clinical MRI scanners but rather to enhance the applicability of MRI, with its tissue contrast capabilities, to a whole new range of medical uses, where employing conventional scanners is impractical or too costly.

ACKNOWLEDGMENTS

The authors express their thanks to Yuval Zur, Assaf Weiss, and the entire development staff of TopSpin Medical (Israel) for their prolonged efforts in this project. We also acknowledge Prof. Gil Navon from Tel-Aviv University, and Prof. Peter Bendel from the Weizmann Institute of Science for providing access to NMR microscopy measurements.

REFERENCES

1. Salibi NM, Brown MA. Clinical MR spectroscopy : first principles. New York: Wiley–Liss; 1998.
2. Blümich B. NMR imaging of materials. Oxford; Oxford University Press; 2000.
3. Burnett LJ, Jackson JA. Sensitivity of NMR detection for external samples. B Am Phys Soc 1980;25:45–45.
4. Eidmann G, Savelsberg R, Blümler P, Blümich B. The NMR MOUSE, a mobile universal surface explorer. J Magn Reson A 1996;122:104–109.
5. McDonald PJ, Newling B. Stray field magnetic resonance imaging. Rep Prog Phys 1998;61:1441–1493.
6. Hurlimann MD, Griffin DD. Spin dynamics of Carr–Purcell–Meiboom–Gill-like sequences in grossly inhomogeneous B_0 and B_1 fields and application to NMR well logging. J Magn Reson 2000;143:120–135.
7. Brown RJS, Chandler R, Jackson JA, Kleinberg RL, Miller MN, Paltiel Z, Prammer MG. History of NMR well logging. Concept Magn Reson 2001;13:335–413.
8. Goelman G, Prammer MG. The CPMG pulse sequence in strong magnetic-field gradients with applications to oil-well logging. J Magn Reson A 1995;113:11–18.
9. Haken R, Blümich B. Anisotropy in tendon investigated in vivo by a portable NMR scanner, the NMR-MOUSE. J Magn Reson 2000;144:195–199.
10. Scharfenecker A, Ardelean I, Kimmich R. Diffusion measurements with the aid of nutation spin echoes appearing after two inhomogeneous radiofrequency pulses in inhomogeneous magnetic fields. J Magn Reson 2001;148:363–366.
11. Meriles CA, Sakellariou D, Heise H, Moule AJ, Pines A. Approach to high-resolution ex situ NMR spectroscopy. Science 2001;293:82–85.
12. Perlo J, Casanova F, Blümich B. 3D imaging with a single-sided sensor: an open tomograph. J Magn Reson 2004;166:228–235.
13. McDonald PJ. Stray field magnetic resonance imaging. Progr Nuclear Magn Reson Spectrosc 1997;30:69–99.
14. Chao SH, Dougherty WM, Garbini JL, Sidles JA. Nanometer-scale magnetic resonance imaging. Rev Sci Instrum 2004;75:1175–1181.
15. Tsuji S, Masumizu T, Yoshinari Y. Magnetic resonance imaging of isolated single liposome by magnetic resonance force microscopy. J Magn Reson 2004;167:211–220.
16. Schneiderman J, Wilensky R, Weiss A, Samouha E, Muchnik L, Chen-Zion M, Ilovitch M, Golan E, Blank A, Flugelman M, Rozenman Y, Virmani R. Diagnosis of thin fibrous cap atheromas by a self-contained intravascular magnetic resonance imaging probe in ex-vivo human aortas and in-situ coronary arteries. J Am Coll Cardiol 2004; in press.
17. Virmani R, Kolodgie FD, Burke AP, Farb A, Schwartz SM. Lessons from sudden coronary death—a comprehensive morphological classification scheme for atherosclerotic lesions. Arterioscl Thromb Vasc 2000;20:1262–1275.
18. Libby P. Atherosclerosis: the new view. Scic Am 2002;286:47–55.
19. Nemirovsky D. Imaging of high-risk plaque. Cardiology 2003;100:160–175.
20. Harpen MD. Influence of skin depth on NMR coil impedance. Phys Med Biol 1988;33:329–337.
21. Satveli R, Moulder JC, Wang B, Rose JH. Impedance of a coil near an imperfectly layered metal structure; the layer approximation. J Appl Phys 1996;79:2811–2821.
22. Buess ML, Petersen GL. Acoustic ringing effects in pulsed nuclear magnetic-resonance probes. Rev Sci Instrum 1978;49:1151–1155.
23. Callaghan PT. Principles of nuclear magnetic resonance microscopy. Oxford: Oxford University Press; 1991.
24. Ott HW. Noise reduction techniques in electronic systems. New York: Wiley; 1988.
25. Dimbylow PJ. Induced current densities from low-frequency magnetic fields in a 2 mm resolution, anatomically realistic model of the body. Phys Med Biol 1998;43:221–230.
26. Nishizawa S, Spreitzer W, Ruoss HO, Landstorfer FM, Hashimoto O. Induced current density in the human body using equivalent sources for low-frequency inhomogeneous fields. Ieice T Electron 2001;E84C:1612–1614.
27. Hoult DI, Richards RE. Signal-to-noise ratio of nuclear magnetic-resonance experiment. J Magn Reson 1976;24:71–85.
28. Balibanu F, Hailu K, Eymael R, Demco DE, Blümich B. Nuclear magnetic resonance in inhomogeneous magnetic fields. J Magn Reson 2000;145:246–258.
29. Zur Y. An algorithm to calculate the NMR signal of a multi spin-echo sequence with relaxation and spin-diffusion. J Magn Reson 2004;171:97–106.
30. Meiboom S, Gill D. Modified spin-echo method for measuring nuclear relaxation times. Rev Sci Instrum 1958;29:688–691.
31. Anferova S, Anferov V, Adams M, Blumler P, Routley N, Hailu K, Kupferschlager K, Mallett MJD, Schroeder G, Sharma S, Blümich B. Construction of a NMR-MOUSE with short dead time. Concept Magn Reson 2002;15:15–25.
32. Toussaint JF, Southern JF, Fuster V, Kantor HL. Water diffusion properties of human atherosclerosis and thrombosis measured by pulse field gradient nuclear magnetic resonance. Arterioscl Thromb Vasc 1997;17:542–546.
33. Yuan C, Kerwin WS. MRI of atherosclerosis. J Magn Reson Imaging 2004;19:710–719.
34. Toussaint JF, Southern JF, Fuster V, Kantor HL. T_2-weighted contrast for nmr characterization of human atherosclerosis. Arterioscl Thromb Vasc 1995;15:1533–1542.
35. Engle J. Low-noise broadband transmit/receive circuit for NMR. J Magn Reson 1980;37:547–549.